ONLINE FIRST

Folia Histochemica et Cytobiologica

ISSN: 0239-8508

e-ISSN: 1897-5631

Therapeutic effect of autophagy induced by rapamycin versus intermittent fasting in animal model of fatty liver

Authors: Sara Adel Hosny, Mohammed Hafez Ahmed Moustafa, Fatma Mahmoud Mehina, Marwa Mohamed Sabry

DOI: 10.5603/fhc.95905

Article type: Original paper

Submitted: 2023-06-06

Accepted: 2023-11-20

Published online: 2023-11-28

ORIGINAL PAPER

Therapeutic effect of autophagy induced by rapamycin versus intermittent fasting in animal model of fatty liver

Sara Adel Hosny, Mohammed Hafez Ahmed Moustafa, Fatma Mahmoud Mehina, Marwa Mohamed Sabry

Department of Histology and Cell Biology, Faculty of Medicine, Cairo University, Egypt

Correspondence address:

Sara Adel Hosny

Department of Histology and Cell Biology, Faculty of Medicine, Cairo University, Kasr Alainy Street, Cairo 11562, Egypt

e-mail: dr.sara_adelh@cu.edu.eg

phone: +02 01005625595

Submitted: 6 June, 2023

Accepted after reviews: 20 November, 2023

Available as AoP: 28 November, 2023

Abstract

Introduction. High-fructose, high-fat diet consumption (HFHF) is one of the primary causes of non-alcoholic fatty liver disease (NAFLD), which is due to impaired beta-oxidation or apolipoprotein secretion by hepatocytes. Activation of autophagy in hepatocytes could be a therapeutic method against hepatic complications. This study was designed to compare effects of rapamycin and intermittent fasting-inducing autophagy in rats with experimentally induced nonalcoholic fatty liver.

Material and methods. Male rats were divided into five groups: C (control, n = 6), the experimental group (EX) subdivided, EXIa (HFHF, n = 6), EXIb (recovery, n = 6), EXII (rapamycin, n = 6) and EXIII (intermittent fasting, n = 6). All rats in the experimental group received HFHF diet for 8 weeks to induce nonalcoholic-fatty liver and obesity. Then, for the next 8 weeks the animals received either a daily oral dose of rapamycin (EXII group) or to intermittent fasting (IF) for 16 hours daily (EXIII group). Blood samples were drawn, and serum TG concentration as well as ALT and AST activities were determined. Hepatic sections were examined by light and electron microscopy. LC3B immunohistochemical staining, morphometric and statistical studies were performed.

Results. Subgroups EXIa (HFHF subgroup) and EXIb (Recovery subgroup) showed marked increase in TG, ALT, and AST levels associated with loss of normal hepatic architecture, cytoplasmic vacuolations and faint LC3B immunoreactivity. Ultrathin sections exhibited many autophagosomes in hepatocytes. On the other hand, rapamycin (EXII) and IF (EXIII) showed significant improvement to a variable extent in comparison to EXI.

Conclusions. It could be concluded that rapamycin and intermittent fasting significantly improved NAFLD-induced changes of liver structure and function by inducing autophagy in hepatocytes.

Keywords: NAFLD; rat; autophagosomes; intermittent fasting; LC3B; rapamycin

Introduction

Autophagy is an intracellular catabolic process where damaged proteins and organelles were degraded in lysosomes. Three types of autophagy are recognized according to the way by which the target substrates are delivered to the lysosomes for degradation: macroautophagy, microautophagy, and chaperone-mediated autophagy [1]. Autophagy decreases liver injury in the non-alcoholic fatty liver by increasing lipophagy, decreasing inflammation, and mitophagy, and preventing megamitochondria formation [2].

Rapamycin, a lipophilic macrolide antibiotic, inhibits the mammalian target of rapamycin (mTOR) [3] which is a serine/threonine protein kinase that forms the catalytic subunit of two protein complexes, known as mTOR Complex 1 (mTORC1) and 2 (mTORC2). mTORC1 increases the production of proteins, nucleotides, and lipids and suppresses catabolic pathways to help cell growth [4]. Rapamycin is mainly used to prevent transplant failure and graft rejection in kidney transplantation [5], cancer therapy [6], and treatment of atherosclerosis (AS) [7].

Intermittent fasting (IF) is a modified fasting regimen used to promote weight loss and may improve metabolic health. Almeneessier and his team [8] reported that matching mealtimes with the circadian clock improves several metabolic parameters. In addition, IF significantly increases the level of *Akkermansia* (one of the gut microbiota) and decreases the level of *Alistipes* (another gut microbiome). An increase in *Akkermansia* species is associated with decreased liver triglyceride accumulation and improved intestinal inflammation, also decreasing in *Alistipes* might improve intestinal inflammation [9]. Recently, it has been discovered that intermittent fasting triggers autophagy by increasing the nuclear localization of transcription factor EB (TFEB), a crucial transcription factor that controls autophagy and the lysosomal machinery. TFEB also increases the transcription of Heat Shock Protein Family B (HSPB8), a group of chaperon proteins that help with the folding, refolding, and recycling of the nascent polypeptide chain in the ER in an ATP-dependent manner. TFEB and HSPB8 activate both general autophagy and chaperone-assisted selective autophagy [10].

Material and Methods

Animals. Thirty male albino rats weighing 180–200 g were included in this study. The animals were bred in the Animal House of the Faculty of Medicine, Cairo University. Each group was

kept in a separate wire cage at room temperature 25°C. All procedures were held according to the ethical guidelines for the care and use of animals at Cairo University (CU-III-F-60-20).

Diets. High-fat, high-fructose diet (FHF) — a diet regimen provides 60% of the total caloric intake from fat and it is prepared by mixing: 55% standard diet (80% carbohydrates, 18% proteins, and 2% fats), 25% beef tallow, 5% roasted peanuts, 5% milk powder, 5% egg, 3% sesame oil and 2% NaCl together with 10% fructose in drinking water [11, 12]. Standard diet contained 80% carbohydrates, 18% proteins, and 2% fats.

Experimental design. Rats were divided into the following groups. Rats in the control group (n = 6) received a standard diet and rats in the experimental groups (n = 24) were fed HFHF diet, water was provided *ad libitum* throughout the experiment. Rats in the experimental (EX) groups were given HFHF diet for 8 weeks to induce both non-alcoholic fatty liver and obesity; thereafter they were subdivided into 4 subgroups. Subgroup EXIa (HFHF subgroup): 6 rats were sacrificed immediately after the 8 weeks of HFHF diet. Subgroup EXIb (Recovery subgroup): 6 rats were left on standard diet without any treatment till the time of sacrification (after another 8 weeks). Subgroup EXII (HFHF + Rapamycin subgroup): 6 rats received a daily single oral dose of rapamycin 2 mg/kg for another 8 weeks then the rats were sacrificed [3]. Subgroup EXIII (HFHF + IF subgroup): 6 rats were subjected to intermittent fasting for 16 hours each day from 4 pm to 8 am with free access to water, and with access to food from 8 am till 4 pm for another 8 weeks, then the rats were sacrificed [13].

By the end of the experimental durations, all the rats were weighed and blood samples were withdrawn from tail veins to measure serum activities of alanine (ALT) and aspartate (AST) transaminases (cat. Number, EEA001 and cat. Number, EEA003, respectively, Thermofisher, Waltham, MA, USA), and triglycerides concentration (cat. Number, EEA028, Thermofisher) in the Department of Medical Biochemistry, Faculty of Medicine, Cairo University, Egypt. The rats were anesthetized by intramuscular injection of ketamine hydrochloride (50 mg/kg) and a ventral midline incision was performed to access the liver. The liver from each animal was fully dissected and weighed, then specimens from the liver tissue were subjected to sampling.

Light microscopic studies. Specimens from the right lobe were fixed in 4% buffered paraformaldehyde to be processed into paraffin blocks. Serial sections at 5 μm thickness were cut using a microtome and mounted on glass slides for staining with hematoxylin and eosin (H&E)

[14]. Other sections were mounted on positively charged slides for immunohistochemistry by the avidin-biotin-peroxidase complex technique using a rabbit monoclonal: Anti-Lipidated LC3B antibody (2 drops or 100 μL for each section) (ab192890; Abcam, Cambridge, UK). Antigen retrieval was done by putting sections into 10 mM citrate buffer (pH 6, 25°C) for 10 min, and then incubated with the primary antibodies overnight at 4°C. Slides were then incubated with secondary antibody (1:1000, Goat Anti-Rat IgG H&L, ab150165, Abcam) was then incubated at 25°C (room temperature) for 20 min. Using Mayer's hematoxylin as a counterstain and diaminobenzidine as a chromogen, immunohistochemical staining was recognized. Human liver tissues were used as positive control for LC3B with brown cytoplasmic and nuclear reactions. We performed negative control sections by skipping the process of using primary antibodies.

Electron microscopic studies. The initial fixation of liver specimens in 2.5% glutaraldehyde in 0.1 M phosphate buffer solution (pH 7.4) for 1–2 h was followed by a post-fixation in 1% osmium tetroxide on sections of the liver measuring about 1 mm^3. The ultrathin sections (60–70 nm) cut with ultramicrotome with diamond knife were placed on copper grids and stained with lead citrate and uranyl acetate to contrast them [15]. In the Faculty of Agricultural Research Center, Cairo University, a transmission electron microscopic (TEM) analysis was carried out using a JEM-1400A microscope (JEOL, Japan) operating at 80 kV.

Western blotting. Western blots were performed according to Ayoubi *et al.* [15] after a quick sonication of small liver samples, lysates made by using protease inhibitor were incubated for 30 min on ice. Protein concentration was measured using BCA reagent (Bicinchoninic Acid Solution, Product No. B9643, SigmaAldrich, Burlington, MA, USA). Alkaline Cu (II) is reduced by proteins to Cu (I) in a concentration-dependent way. A very selective chromogenic agent for copper (I), bicinchoninic acid forms a compound with a maximum absorbance at 562 nm. This characteristic causes the resulting 562 nm absorbance to be directly proportional to the protein concentration. A protein standard is utilized, which is bovine serum albumin. Equal protein aliquots of the supernatants from the spun-down lysates were subjected to SDS-PAGE and immunoblot analysis. The GeneDireX BLUelf prestained protein ladder (catalog number PM008-0500) was utilized. The primary antibody against LC3 protein (1:1000, rabbit polyclonal antibody, ab48394, Abcam). Large polyacrylamide gels with a 5–16% gradient was used for the immunoblots, and they were subsequently transferred to nitrocellulose membranes. Ponceau

staining was utilized to view the proteins on the blots, which were then scanned at 300 dpi using a standard flatbed scanner to display alongside each immunoblot. Antibodies were incubated O/N at 4°C with 5% bovine serum albumin in TBS with 0.1% Tween 20 (TBST) after blots were blocked with 5% milk for 1 h. Then the slides were incubated with peroxidase-conjugated secondary antibody for 1 h at room temperature at a dilution of 0.2 μg/mL in TBST with 5% milk, followed by three TBST washes. Before detection using HyBlot CL autoradiography films (cat. Number 1159T41, Denville, NJ, USA), membranes were treated with ECL (cat. Number 32106, Pierce, Waltham, MA, USA).

Morphometric study. Slides were observed using a light microscope. Ten non-overlapping fields from different sections of each rat group were examined to measure: mean area % of LC3B immunopositive area (100×) and mean number of autophagosomes in ultrathin sections at the magnification of 16000×. The Leica Qwin 500 C image analyzer computer system (Cambridge, UK) was used to collect the data. The image analyzer was made up of an Olympus color video camera, a colored monitor, an IBM personal computer's hard drive attached to the microscope, and Leica Qwin 500 C software. To automatically convert the measurement units (pixels) generated by the image analyzer program into real micrometer units, the image analyzer was first calibrated.

Statistical analysis. SPSS software version 16 was used to analyze the measurements (SPSS, Chicago, IL, USA). ANOVA and the *post hoc* Tukey test were used to compare the differences between the various groups. Means and standard deviation (SD) were used to express the results. When the P-value was 0.05 or less, the differences were deemed statistically significant.

Results

High-fat, high-fructose diet (HFHF) increases body and liver weight

Body and liver weights of rats in experimental subgroups EXIa (HFHF subgroup) and EXIb (Recovery subgroup) was significantly increased when compared to control and experimental groups EXII (HFHF + Rapamycin subgroup) and EXIII (HFHF + IF subgroup) (Table 1). The body weight in subgroups EXII (HFHF + Rapamycin subgroup) and EXIII (HFHF + IF subgroup) exhibited a significant increase in comparison with the control group. On the other

hand, the liver weight of EXII (HFHF + Rapamycin subgroup) and EXIII (HFHF + IF subgroup) subgroups demonstrated no significant difference when compared with that of the control group. No significant difference between subgroups EXII (HFHF + Rapamycin subgroup) and EXIII (HFHF + IF subgroup) was found.

High-fat, high-fructose diet increased serum activities of liver marker enzymes and triglycerides concentration

The experimental subgroups EXIa (HFHF subgroup) and EXIb (Recovery subgroup) demonstrated a significant increase in serum activities of ALT and AST, and serum triglycerides concentration when compared to the control group (Table 1). Values for EXII (HFHF + Rapamycin) and EXIII (HFHF + IF) subgroups showed a statistically significant decrease in comparison to EXIa, (HFHF) and EXIb (Recovery) subgroups with significant differences between EXII and EXIII subgroups.

Hematoxylin and eosin staining reveals destruction of hepatic architecture induced by HFHF diet

Histological of sections of the liver in the control rat group revealed a normal hepatic pattern. Liver in subgroups EXIa (HFHF subgroup) and EXIb (Recovery subgroup) revealed loss of the normal radiating pattern of hepatocytes (Fig. 1). Hepatic cells appeared disorganized, enlarged and with vacuolated cytoplasm. Some cells had dark pyknotic nuclei and others had vacuolated nuclei. The cytoplasm of hepatocytes exhibited either multiple vacuoles or a single large vacuole occupying the whole cytoplasm. Blood sinusoids appeared dilated and congested (Fig. 1).

On the contrary, liver of rats in subgroups EXII (HFHF + Rapamycin) and EXIII (HFHF + IF) exhibited plates of hepatocytes radiating from the central vein. Hepatocytes were average in size with pale nuclei. The cells had eosinophilic cytoplasm (Fig. 1).

Toluidine blue staining of the semithin sections demonstrated amelioration of hepatic damage induced by HFHF in the liver of rats treated with rapamycin and intermittent fasting

Examination of liver sections of the control rats exhibited hepatocytes having pale nuclei with the prominent nucleolus, thin nuclear membrane, and granular cytoplasm with clear thin cell boundaries (Fig. 2A). Hepatocytes of the subgroup EXIa (HFHF subgroup) revealed irregular

vacuoles compressing the nucleus (Fig. 2B). However, liver in subgroup EXIb (Recovery subgroup) revealed marked disorganization of the hepatocyte. Many hepatocytes had no nuclei and few cells showed dark shrunken nuclei with thick nuclear envelopes (Fig. 2C). Livers in EXII (HFHF + Rapamycin) and EXIII (HFHF + IF) subgroups contained hepatocytes having regular cell boundaries, pale nuclei with the prominent nucleolus, and clear nuclear envelope. Few hepatocytes had small vacuoles in the cytoplasm (Fig. 2D, E).

Autophagy detection by LC3B immunostaining

The liver sections of control rats showed a widespread membranous reaction for LC3B, but some hepatocytes revealed also positive cytoplasmic immunoreactivity to LC3B (Fig. 3B). Only few cells in the subgroups EXIa (HFHF subgroup) and EXIb (Recovery subgroup) exhibited faint cytoplasmic LC3B immunoreactivity (Fig. 3C, D). The cytoplasm of the hepatocytes in the subgroups EXII (HFHF + Rapamycin subgroup) and EXIII (HFHF + IF subgroup) demonstrated extensive immunoreactivity with some nuclear reaction (Fig. 3E, F).

Changes in LCII/LCI ratio in all studied groups

In our experiment, the mean values of LCII/LCI ratio in subgroups EXIa (HFHF subgrou0p) and EXIb (Recovery subgroup) revealed lower values comparable to that of the control group (Fig. 5 A,B). The EXII (HFHF + Rapamycin) and EXIII (HFHF + IF) subgroups showed a significant increase when compared with EXIa (HFHF subgroup) and EXIb (Recovery subgroup) subgroups and the control group. Furthermore, no statistically significant difference was found between subgroups EXII (HFHF + Rapamycin) and EXIII (HFHF + IF).

Ultrastructure of hepatocytes in the rat liver

Electron microscopic examination of control rats revealed hepatocytes with euchromatic nucleus, prominent nucleolus and regular nuclear envelope. The cytoplasm had numerous mitochondria, rough endoplasmic reticulum (rER), and glycogen granules (Fig. 4 A, B). Subgroups EXIa (HFHF subgroup) and EXIb (Recovery subgroup) showed hepatocytes with coarse chromatin attached to the thick nuclear membrane giving the fuzzy appearance. Multiple lipid droplets were seen in the cytoplasm associated with dilated rough endoplasmic reticulum (rER) cisternae and shrunken mitochondria (Fig. 4C, D). Subgroups EXII (HFHF + Rapamycin) and EXIII (HFHF +

IF) exhibited hepatocytes with euchromatic nuclei, prominent nucleolus, and regular nuclear membrane. Many autophagosomes were seen in the cytoplasm as double membrane structures and some contained lipids. The forming membrane (phagophore) and phagolysosome with digested materials were present demonstrated in the cytoplasm of some cells. The cytoplasm revealed large number of mitochondria with rER cisternae (Fig. 4 E–K).

Morphometric assessment of LC3B immunopositive area and number of autophagosomes in studied groups

The mean percentage area of LC3B immunopositive area and number of autophagosomes in ultrathin sections in subgroups EXIa (HFHF subgroup) and EXIb (Recovery subgroup) revealed a significant decrease compared to those of the control group (Fig. 5C, D). On the contrary, subgroups EXII (HFHF + Rapamycin) and EXIII (HFHF + IF) values showed a significant increase when compared with EXIa (HFHF) and EXIb (Recovery subgroup) subgroups and the control group. Furthermore, a statistically significant decrease in EXIII (HFHF + IF) subgroup in comparison with EXII (HFHF + Rapamycin subgroup) was noted (Fig. 5C, D).

Discussion

Autophagy is an intracellular catabolic process that allows the degradation of damaged proteins and organelles in lysosomes. Autophagy consists of three major steps: autophagosome formation, fusion with the lysosome, and finally degradation [17]. It was reported by Khambu *et al.* that impaired autophagy decreases the clearance of excessive lipid droplets in hepatocytes that lead to the development of non-alcoholic fatty liver (NAFLD) [18].

The current study was designed to compare the effects of rapamycin and intermittent fasting regarding their ability to induce autophagy in the liver of HFHF-exposed male rats.

In the HFHF (EXIa) and Recovery (EXIb) subgroups, body and liver weights revealed a statistically significant increase after HFHF diet when compared with control rats which received standard diet. These results coincident with Gao *et al.* [19] where both body and liver weight increased in rats received HFD and developed fatty liver. This increase is attributed to fat deposition in adipose tissue and hepatocyte [20]. In addition, subgroups EXIa (HFHF subgroup)

and EXIb (Recovery subgroup) exhibited a significant increase in mean values of ALT and AST serum levels when compared with control group. These enzymes are normally present in the cytoplasm of hepatocytes. When hepatocytes are damaged and their permeability increases, the enzymes were released into the plasma indicating liver cell injury. This agreed with another study done by Albadawy *et al.* [21].

Moreover, TG levels were also significantly higher than the control group values. It was reported by Tomizawa *et al.* that hypertriglyceridemia is most prevalent among patients with NAFLD [22].

Hematoxylin and eosin sections after HFHF diet in EXIa (HFHF subgroup) and EXIb (Recovery subgroup) revealed loss of the normal radiating pattern of hepatocytes. This is explained as a result of oxidative damage of hepatocellular proteins or a result of necrotic changes in hepatocytes that lead to irregularity in the orientation of the hepatocyte plates and disturbing hepatic architecture. Ballooning of hepatocytes appeared with vacuolated cytoplasm confirmed by the presence of electron lucent lipid droplets by EM. The large size and ballooning of hepatocytes are due to the distraction of cell cytoskeleton and severe cell injury [23].

Vacuolation in the cytoplasm may have the form of macro- or microvesicular steatosis. Macrovesicular steatosis is due to abnormalities in the metabolism, production, or transfer of lipids [24]. Meanwhile, microvesicular steatosis is associated with defective beta-oxidation of fatty acids [25]. Furthermore, cytoplasmic vacuolation was assigned to lipid peroxidation because of oxidative stress that damages the cell membrane and membranes of cell organelles leading to an increase in their permeability and subsequent disturbance of the ion’s concentrations in the cytoplasm and cell organelles [26].

Kořínková *et al.* explained the pathogenesis of NAFLD by the “two-hit” hypothesis [27]. The first hit is a direct cytotoxic effect due to excessive fat accumulation, while the second hit is an indirect cytotoxic effect due to the peroxidation of fatty acids. Excessive fatty acids in the liver make the liver more vulnerable to injury to stressors such as reactive oxygen species (ROS), adipokines, and cytokines than a normal liver. The regenerative capacity of a fatty liver is also impaired.

Dark pyknotic nuclei were observed in some hepatocytes, confirmed by condensation of chromatin which is due to the impaired antioxidant activity of the cells, making them more vulnerable to the effects of reactive oxygen species [28]. However, other cells displayed

vacuolated nuclei (glycogenated nuclei) due to the accumulation of glycogen in the nuclei, this is a common finding in liver biopsies with diabetes, Wilson disease, and NAFLD [26].
In addition, dilatation of central veins and blood sinusoids were attributed to inflammatory changes or ischemia and hypoxia following a high-fat diet [29].

When the phagophore membranes expand, a cleaved form of the protein MAP1LC3B (LC3BI), is diffusely expressed in the cytoplasm and conjugates to the lipid phosphatidylethanolamine. The protein is now termed LC3B-II, and through its lipid conjugate integrates into the phagophore membrane. Both the inner and outer membranes of the autophagosome contain LC3B-II [30]. LC3B is a widely used autophagosome marker as the amount of LC3B-II reflects the number of autophagosomes but LC3B cannot differentiate between LC3BI and LC3BII so a western blot was done to differentiate between both types of the LC3B protein.

The mean percentage area of LC3B immunoreactivity and the ratio of LC3B-I to LC3B-II in Western blots were significantly lower in the EXIa (HFHF subgroup) and EXIb (Recovery subgroup) subgroups than the control group and EXII (HFHF + Rapamycin subgroup) and EXIII (HFHF + IF subgroup), indicating weak autophagic activity in these groups. This finding corresponds to the data of Korovila *et al.* who reported that fat accumulation in the liver due to a high-fat diet is associated with a failure of autophagy and leads to the disturbance of proteostasis. This might further contribute to lipid droplet stabilization and accumulation [31].

These findings were enforced by the number of autophagosomes in EM sections which were lower than those in the control group and EXII (HFHF + Rapamycin subgroup) and EXIII (HFHF + IF subgroup) subgroups. Recently, it has been reported that the unfolded protein response (UPR) and autophagy have been shown to share common regulatory pathways [32]. The spliced form of XBP1(X-box binding protein 1; sXBP1), a transcription factor necessary for UPR activation, binds to the promoter region and activates the expression of transcription factor EB (TFEB). This interaction is reduced in the steatotic hepatic tissue [32].

In the EXII (HFHF + Rapamycin subgroup), where rapamycin was given for 8 weeks after 8 weeks of the HFHF diet, body and liver weights returned to almost normal values that were significantly lower than those of the EXI group. Chang *et al.* [33] reported that when rapamycin is given to mice that were fed on HFHF, body, and liver weights were significantly decreased. They referred these findings to the ability of rapamycin to reduce the number of large

adipocytes, potentially due to its ability to promote fat combustion. Rapamycin reduced expressions of most adipogenic genes including PPARγ, C/EBPa, FAS, aP2, adipsin, and ADD1/SREBP1c, which affect lipogenesis. It reduced triacylglycerol accumulation and adipogenesis. Furthermore, Pena-Leon *et al.* [34] reported that the mTOR pathway plays a role in the regulation of food intake and energy homeostasis.

In addition, the EXII (HFHF + Rapamycin subgroup) group exhibited a decline in the mean values of ALT and AST towards the normal level which is significantly lower than those of EXI. Rapamycin has been also found to decrease levels of acetyl-coenzyme A carboxylase fatty acid synthase (FASN) and stearoyl-CoA desaturase 1 (SCD-1). Thus, Rapamycin could efficiently protect from HFHF-induced hepatic steatosis and liver injury in mice with NAFLD [35].

Liver sections of rats from EXII (HFHF + Rapamycin subgroup) revealed preserved radiating patterns of hepatocytes from the central vein. Hepatocytes were of average size with a pale nucleus which is confirmed by examination of ultrathin sections. The capacity of rapamycin to cause lipid droplet autophagy explained the therapeutic effect of rapamycin on NAFLD. It was reported by Yu and his team [3] that rapamycin is a typical mTOR inhibitor. Inhibition of the mTOR pathway activates the intracellular ULK1 complex, which triggers its affinity for ATG13 and ATG17 to form a multi-protein complex. This results in the recruitment of other ATG proteins to form autophagosomes [36].

Ma *et al.* [37] verified that *de novo* lipogenesis (DNL) accounts for 25% of the total hepatic lipids and plays an important role in NAFLD development. DNL is mainly controlled by a lipogenic transcription factor, sterol regulatory element-binding protein1 (SREBP1). It was found that the expression of SREBP1 was regulated by mTOR. Moreover, Feng and coworkers [38] reported that mTORC1 reduced the transcriptional activity of transcription factor EB (TFEB) that has been identified as a master regulator of lysosomal function. So, inhibition of mTORC1 by rapamycin can protect against fatty liver and restore the normal histological picture of hepatic section [39].

Many autophagosomes have been demonstrated in the cytoplasm of mammalian cells as double-membrane structures with some containing lipids, which was reported by Periyasamy-Thandavan *et al.* [40]. This was reinforced by the morphometric studies where the mean numbers

of autophagosomes were significantly higher in subgroup EXII (HFHF + Rapamycin subgroup) as compared to control and subgroups EXI (HFHF subgroup) and EXIII (HFHF + IF subgroup).

LC3B-stained sections of EXII (HFHF + Rapamycin subgroup) showed strong positive cytoplasmic reaction with a significant increase in mean percentage of the immunoreactive area and LC3B-II to LC3B-I ratio in western blot as compared to subgroup EXI and EXIII (HFHF + IF subgroup) and control group indicating effective phagosome formation. Similarly to our hepatic study, Diao *et al.* [41] noticed increased expression of LC3B in immunostained renal sections after intraperitoneal injection of rapamycin.

In subgroup EXIII (HFHF + IF subgroup), body and liver weights returned to almost normal values; they were significantly lower than those of the EXI subgroup. In a study performed in 2020, Harahap *et al.* [42] reported a similar decrease in body weight after intermittent fasting as it decreases body weight by decreasing leptin level as well as elevation in adiponectin level.

EXIII (HFHF + IF subgroup) exhibited a decline of ALT and AST serum activities towards the normal level. This decrease in the liver marker enzymes activity could be explained by decreased destruction of hepatocytes [43]. In addition, the TG serum level in this subgroup was significantly lower than EXI and EXII. It was reported that IF results in a metabolic switch (switch from glucose to fatty acid-derived ketones) leading to a breakdown of triglycerides into fatty acids and glycerol and conversion of fatty acids to ketone bodies in the liver. During fasting, fatty acids and ketone bodies provide energy to cells and tissues [44].

Liver sections of rats from EXIII (HFHF + IF subgroup) revealed nearly normal hepatic architecture, as de Castro-de-Paiva *et al.* [45] have reported that intermittent fasting after 2 months of HF diets decreased steatosis and hepatocytic vacuolations. Autophagy is stimulated in response to food withdrawal.

IF has a potential role in treating a variety of liver diseases, including non-alcoholic fatty liver disease, drug-induced liver injury, viral hepatitis, hepatic fibrosis, and hepatocellular carcinoma through stimulating autophagy by influencing the metabolism of energy and oxygen radicals as well as cellular stress response systems, protecting hepatocytes from genetic and environmental factors [46]. This improvement also was detected by examination of ultrathin sections revealing hepatocytes with the euchromatic nucleus and regular nuclear membrane.

Some autophagosomes were seen in the cytoplasm with phagophore and phagolysosome were noticed.

The appearance of autophagosomes approves the ability of IF to stimulate autophagy. This was reinforced by the morphometric study where the number of autophagosomes was significantly increased in subgroup EXIII (HFHF + IF subgroup) as compared to subgroup EXI and the control group. However, the number was significantly lower than in the EXII group. Intermittent fasting stimulates autophagy in EXIII (HFHF + IF subgroup) by activation of the adenosine monophosphate (AMP)-activated protein kinase (AMPK)/mammalian target of rapamycin (mTOR) pathway and enhances lysosome function by upregulating transcription factor (TFEB) expression [47].

EXIII (HFHF + IF subgroup) showed strong + ve cytoplasmic immunoreaction to LC3B with increased mean percentage area when compared to subgroup EXI and control group, but it was significantly lower than EXII. Similarly, Ebrahim *et al.* [48] noticed an increase in LC3B expression in the cerebellar cortex of mice submitted for IF after 12 weeks of a high-fat diet.

In the western blot, LC3B-II to LC3B-I ratio was significantly higher than the control and EXIa (HFHF subgroup) and EXIb (Recovery subgroup) subgroups. This means that LCI was converted to LCII and was incorporated into the autophagosome membrane. The same finding was reported by Yuan *et al.* [48] when IF was used to induce autophagy in spinal cord injury in rats.

It could be concluded that obesity and NAFLD are inevitable consequences of HFHF diet. Both IF and rapamycin have an effective role in alleviating hepatic damage from HFHF diet through their autophagy induction ability. However, rapamycin showed better improvement in hepatic tissue damage compared to IF as proved by the histological and morphometric results of this study.

Article information

Data availability statement

All data used in the current study are available from the corresponding author upon reasonable request.

Ethics statement

This study followed international guidelines for the use and care of laboratory animals and was approved (CU-III-F-60-20) by the Institutional Animal Care and Use Committee of Cairo University (IACUC).

Author contributions

Conceptualization: Hosny S.A., Moustafa M.H.A., Mehina F.M., Sabry M.M., Methodology and validation: Hosny S.A., Moustafa M.H.A., Mehina F.M., Sabry M.M. Writing — original draft and figure preparation: Hosny S.A., Mehina F.M., Writing — review and editing: Hosny S.A., Moustafa M.H.A., Mehina F.M., Sabry M.M., Supervision: Moustafa M.H.A., Hosny S.A.
All authors reviewed the manuscript.

Funding

No funding.

Acknowledgments

We would like to thank Professor Laila Ahmed Rashed, Department of Biochemistry, Faculty of Medicine, Cairo University, Egypt performed biochemical and serological procedures. Mr. Kareem Hassan technician at Medical Histology and Cell Biology Department contributed to specimens' preparation.

Conflict of interest

The authors have declared that they have no competing interests.

References

1. Mao YQ, Yu F, Wang J, et al. Autophagy: a new target for nonalcoholic fatty liver disease therapy. Hepat Med. 2016; 8: 27–37, doi: 10.2147/hmer.s98120, indexed in Pubmed: 27099536.

2. Allaire M, Rautou PE, Codogno P, et al. Autophagy in liver diseases: Time for translation? J Hepat. 2019; 70(5): 985–998, doi: 10.1016/j.jhep.2019.01.026, indexed in Pubmed: 30711404.

3. Yu X, Zhang L, Lu H, et al. Rapamycin protects against hepatic injury in streptozotocin-induced diabetic rats by enhancing autophagy. Int J Clin Exp Med. 2019; 12(9): 11383–11393.

4. Saxton R, Sabatini D. mTOR Signaling in Growth, Metabolism, and Disease. Cell. 2017; 168(6): 960–976, doi: 10.1016/j.cell.2017.02.004, indexed in Pubmed: 28283069.

5. Hahn D, Hodson EM, Hamiwka LA, et al. Target of rapamycin inhibitors (TOR-I; sirolimus and everolimus) for primary immunosuppression in kidney transplant recipients. Cochrane Database Syst Rev. 2019; 12(12): CD004290, doi: 10.1002/14651858.cd004290.pub3, indexed in Pubmed: 31840244.

6. Tian T, Li X, Zhang J. mTOR Signaling in Cancer and mTOR Inhibitors in Solid Tumor Targeting Therapy. Int J Mol Sci. 2019; 20(3): 755, doi: 10.3390/ijms20030755, indexed in Pubmed: 30754640.

7. Palavra F, Robalo C, Reis F. Recent advances and challenges of mTOR inhibitors use in the treatment of patients with Tuberous Sclerosis Complex. Oxid Med Cell Longev. 2017; 2017: 9820181, doi: 10.1155/2017/9820181, indexed in Pubmed: 28386314.

8. Almeneessier AS, Pandi-Perumal S, BaHammam A. Intermittent fasting, insufficient sleep, and circadian rhythm: interaction and effects on the cardiometabolic system. Curr Sleep Medicine Rep. 2018; 4(3): 179–195, doi: 10.1007/s40675-018-0124-5.

9. Li L, Su Y, Li F, et al. The effects of daily fasting hours on shaping gut microbiota in mice. BMC Microbiol. 2020; 20(1): 65, doi: 10.1186/s12866-020-01754-2, indexed in Pubmed: 32209070.

10. Mukai R, Zablocki D, Sadoshima J. Intermittent fasting reverses an advanced form of cardiomyopathy. J Am Heart Assoc. 2019; 8(4): e011863, doi: 10.1161/jaha.118.011863, indexed in Pubmed: 30773085.

11. Ragab SM, Omar HE, Kh S. Hypolipidemic and antioxidant effects of phytochemical compounds against hepatic steatosis induced by high-fat high sucrose diet in rats. Archives of Biomedical Sciences. 2014; 2(1): 1–10.

12. van Herck M, Vonghia L, Francque S. Animal models of nonalcoholic fatty liver disease — a starter's guide. Nutrients. 2017; 9(10): 1072, doi: 10.3390/nu9101072, indexed in Pubmed: 28953222.

13. Aouichat S, Chayah M, Bouguerra-Aouichat S, et al. Time-restricted feeding improves body weight gain, lipid profiles, and atherogenic indices in cafeteria-diet-fed rats: role of browning of inguinal white adipose tissue. Nutrients. 2020; 12(8): 2185, doi: 10.3390/nu12082185, indexed in Pubmed: 32717874.

14. Kiernan JK. Histological and histochemical methods. In: Theory and practice. 3rd ed. Arnold Publisher, London, New York, and New Delhy 2001: 111–162.

15. Woods AE, Stirling JW. Electron microscopy. In: Bancroft JD, Gamble M. ed. Theory and practice of histological techniques, 6th ed. Churchill Livingstone Elsevier, Edinburgh 2008: 601–636.

16. Ayoubi R, McPherson PS, Laflamme C. Antibody Screening by Immunoblot. https://zenodo.org/records/5717510 (6.05.2023).

17. Cui F, Hu H, Guo J, et al. The effect of autophagy on chronic intermittent hypobaric hypoxia ameliorating liver damage in metabolic syndrome rats. Front Physiol. 2020; 11: 13, doi: 10.3389/fphys.2020.00013, indexed in Pubmed: 32082187.

18. Khambu B, Yan S, Huda N, et al. Autophagy in non-alcoholic fatty liver disease and alcoholic liver disease. Liver Res. 2018; 2(3): 112–119, doi: 10.1016/j.livres.2018.09.004, indexed in Pubmed: 31123622.

19. Gao H, Zhou L, Zhong Y, et al. Kindlin-2 haploinsufficiency protects against fatty liver by targeting Foxo1 in mice. Nat Commun. 2022; 13(1): 1025, doi: 10.1038/s41467-022-28692-z, indexed in Pubmed: 35197460.

20. Qian Ll, Wu L, Zhang L, et al. Serum biomarkers combined with ultrasonography for early diagnosis of non-alcoholic fatty liver disease confirmed by magnetic resonance spectroscopy. Acta Pharmacol Sin. 2019; 41(4): 554–560, doi: 10.1038/s41401-019-0321-x, indexed in Pubmed: 31776449.

21. Albadawy R, Hasanin A, Agwa S, et al. Rosavin Ameliorates Hepatic Inflammation and Fibrosis in the NASH Rat Model via Targeting Hepatic Cell Death. Int J Mol Sci. 2022; 23(17): 10148, doi: 10.3390/ijms231710148, indexed in Pubmed: 36077546.

22. Tomizawa M, Kawanabe Y, Shinozaki F, et al. Triglyceride is strongly associated with nonalcoholic fatty liver disease among markers of hyperlipidemia and diabetes. Biomed Rep. 2014; 2(5): 633–636, doi: 10.3892/br.2014.309, indexed in Pubmed: 25054002.

23. Ore A, Ugbaja R, Adeogun A, et al. An albino mouse model of nonalcoholic fatty liver disease induced using high-fat liquid “Lieber-DeCarli” diet: a preliminary investigation. Porto Biomed J. 2020; 5(4): e071, doi: 10.1097/j.pbj.0000000000000071, indexed in Pubmed: 32734012.

24. Reddy JK, Rao MS. Lipid Metabolism and Liver Inflammation. II. Fatty liver disease and fatty acid oxidation. Am J Physiol Gastrointest Liver Physiol. 2006; 290(5): G852–G858, doi: 10.1152/ajpgi.00521.2005, indexed in Pubmed: 16603729.

25. Rives C, Fougerat A, Ellero-Simatos S, et al. Oxidative Stress in NAFLD: Role of Nutrients and Food Contaminants. Biomolecules. 2020; 10(12): 1702, doi: 10.3390/biom10121702, indexed in Pubmed: 33371482.

26. Okasha E, Hassan N, Soliman G, et al. Histological, immunohistochemical, and biochemical study of experimentally induced fatty liver in adult male albino rat and the possible protective role of pomegranate. J Microsc Ultrastruct. 2018; 6(1): 44–55, doi: 10.4103/jmau.jmau_5_18, indexed in Pubmed: 30023266.

27. Kořínková L, Pražienková V, Černá L, et al. Pathophysiology of NAFLD and NASH in experimental models: the role of food intake regulating peptides. Front Endocrinol (Lausanne). 2020; 11: 597583, doi: 10.3389/fendo.2020.597583, indexed in Pubmed: 33324348.

28. Ao Na, Yang J, Wang X, et al. Glucagon-like peptide-1 preserves non-alcoholic fatty liver disease through inhibition of the endoplasmic reticulum stress-associated pathway. Hepatol Res. 2016; 46(4): 343–353, doi: 10.1111/hepr.12551, indexed in Pubmed: 26147696.

29. Abdeen M, Zaghloul D, Saleh R, et al. Histomorphometric evidence of hepatic recovery of rats fed repeatedly heated palm oil. Egyptian Journal of Histology. 2022; 45(1): 115–124, doi: 10.21608/ejh.2021.57674.1415.

30. Martinet W, Schrijvers DM, Timmermans JP, et al. Immunohistochemical analysis of macroautophagy. Autophagy. 2014; 9(3): 386–402, doi: 10.4161/auto.22968.

31. Korovila I, Höhn A, Jung T, et al. Reduced liver autophagy in high-fat diet induced liver steatosis in New Zealand obese mice. Antioxidants. 2021; 10(4): 501, doi: 10.3390/antiox10040501, indexed in Pubmed: 33804819.

32. Zhang Z, Qian Q, Li M, et al. The unfolded protein response regulates hepatic autophagy by sXBP1-mediated activation of TFEB. Autophagy. 2020; 17(8): 1841–1855, doi: 10.1080/15548627.2020.1788889.

33. Chang GR, Chiu YS, Wu YY, et al. Rapamycin protects against high fat diet–induced obesity in C57BL/6J mice. J Pharmacol Sci. 2009; 109(4): 496–503, doi: 10.1254/jphs.08215fp, indexed in Pubmed: 19372632.

34. Pena-Leon V, Perez-Lois R, Seoane L. mTOR pathway is involved in energy homeostasis regulation as a part of the gut–brain axis. Int J Mol Sci. 2020; 21(16): 5715, doi: 10.3390/ijms21165715, indexed in Pubmed: 32784967.

35. Zhao R, Zhu M, Zhou S, et al. Rapamycin-Loaded mPEG-PLGA nanoparticles ameliorate hepatic steatosis and liver injury in non-alcoholic fatty liver disease. Front Chem. 2020; 8: 407, doi: 10.3389/fchem.2020.00407, indexed in Pubmed: 32548088.

36. Alers S, Löffler A, Wesselborg S, et al. Role of AMPK-mTOR-Ulk1/2 in the regulation of autophagy: cross talk, shortcuts, and feedbacks. Molecular and Cellular Biology. 2023; 32(1): 2–11, doi: 10.1128/mcb.06159-11, indexed in Pubmed: 22025673.

37. Ma N, Wang YK, Xu S, et al. PPDPF alleviates hepatic steatosis through inhibition of mTOR signaling. Nat Commun. 2021; 12(1): 3059, doi: 10.1038/s41467-021-23285-8, indexed in Pubmed: 34031390.

38. Feng J, Qiu S, Zhou S, et al. mTOR: a potential new target in nonalcoholic fatty liver disease. Int J Mol Sci. 2022; 23(16): 9196, doi: 10.3390/ijms23169196, indexed in Pubmed: 36012464.

39. Gosis B, Wada S, Thorsheim C, et al. Inhibition of nonalcoholic fatty liver disease in mice by selective inhibition of mTORC1. Science. 2022; 376(6590), doi: 10.1126/science.abf8271.

40. Periyasamy-Thandavan S, Jiang M, Schoenlein P, et al. Autophagy: molecular machinery, regulation, and implications for renal pathophysiology. Am J Physiol Renal Physiol. 2009; 297(2): F244–F256, doi: 10.1152/ajprenal.00033.2009, indexed in Pubmed: 19279132.

41. Diao C, Wang L, Liu H, et al. Aged kidneys are refractory to autophagy activation in a rat model of renal ischemia-reperfusion injury. Clin Interv Aging. 2019; Volume 14: 525–534, doi: 10.2147/cia.s197444, indexed in Pubmed: 30880933.

42. Harahap H, Esa A, Erny K. The Effect of Intermitent Fasting (Time Restriction Feeding) on Body Weight, Aspartate Transaminase and Alkaline Transaminase in Sprague Dawley Rats. https://www.researchgate.net/publication/345039438_The_Effect_of_Intermitent_Fasting_Time_Restriction_Feeding_on_Body_Weight_Aspartate_Transaminase_and_Alkaline_Transaminase_in_Sprague_Dawley_Rats (6.05.2023).

43. Yin C, Li Z, Xiang Y, et al. Effect of intermittent fasting on non-alcoholic fatty liver disease: systematic review and meta-analysis. Front Nutr. 2021; 8: 709683, doi: 10.3389/fnut.2021.709683, indexed in Pubmed: 34322514.

44. Ahmed K, Arisha A, Sharsher S. The influence of intermittent fasting regimens on the regulatory mechanisms of metabolic health. Zagazig Veterinary Journal. 2021; 49(1): 56–66, doi: 10.21608/zvjz.2021.27440.1112.

45. Castro-de-Paiva Pde, Marinho T, Mandarim-de-Lacerda C, et al. Intermittent fasting, high-intensity interval training, or a combination of both have beneficial effects in obese mice with nonalcoholic fatty liver disease. J Nutr Biochem. 2022; 104: 108997, doi: 10.1016/j.jnutbio.2022.108997, indexed in Pubmed: 35331900.

46. Ma YN, Jiang X, Tang W. Influence of intermittent fasting on autophagy in the liver. Biosci Trends. 2023; 17(5): 335–355, doi: 10.5582/bst.2023.01207, indexed in Pubmed: 37661370.

47. Yuan W, He X, Morin D, et al. Autophagy induction contributes to the neuroprotective impact of intermittent fasting on the acutely injured spinal cord. J Neurotrauma. 2021; 38(3): 373–384, doi: 10.1089/neu.2020.7166, indexed in Pubmed: 33076741.

48. Ebrahim HA, El-Gamal R, Sherif RN. Intermittent fasting attenuates high-fat diet-induced cerebellar changes in rats: involvement of tnf-α, autophagy, and oxidative stress. Cells Tissues Organs. 2021; 210(5-6): 351–367, doi: 10.1159/000519088, indexed in Pubmed: 34551416.

Table 1. Body and liver weight and serum biochemical indices of liver function in all rat groups

	Control group	HFHF subgroup	Recovery subgroup	HFHF + Rap subgroup	HFHF + IF subgroup
Body weight [g]	216 ± 5.7	335.5 ± 9.8*	327 ± 5.7*	257.8 ± 2.1$^{*\#}$	250.4 ± 3.4$^{*\#}$
Liver weight [g]	10.08 ± 0.07	13.9 ± 0.25*	13.7 ± 0.16*	9.98 ± 0.15$^{\#}$	10.2 ± 0.36$^{\#}$
Liver/body weight [%]	4.82 ± 0.39	4.26 ± 0.43	4.4 ± 0.55	3.67 ± 0.36$^{*\#}$	3.81 ± 0.37*
Serum TG concentration [mg/dL]	59.5 ± 4.4	98.8 ± 4.5*	93.1 ± 5.1*	71.5 ± 4.8$^{\#}$	64.3 ± 4.2^{0}
Serum ALT activity [U/L]	54.8 ± 2.9	115.2 ± 3.1*	116.8 ± 4.6*	61.9 ± 3.3$^{\#}$	74.5 ± 2.6^{0}
Serum AST activity [U/L]	65.7 ± 1.7	130.5 ± 1.6*	132.8 ± 2.6*	75.1 ± 1.5$^{\#}$	90 ± 2.4^{0}

The values express mean value ± standard deviation. *Significant difference compared to the control group, $P < 0.05$. $^{\#}$Significantly different from subgroups EXIa (HFHF subgroup) &EXIb, $P < 0.05$; ^{0} Significantly different from control group and subgroups EXIa (HFHF subgroup), EXIb (Recovery subgroup) and EXII (HFHF + IF subgroup, $P < 0.05$. Abbreviations: ALT — Alanine transaminase; AST — Aspartate transaminase; HFHF — high fat high fructose; IF — intermittent fasting; Rap — rapamycin; TG — triglycerides.

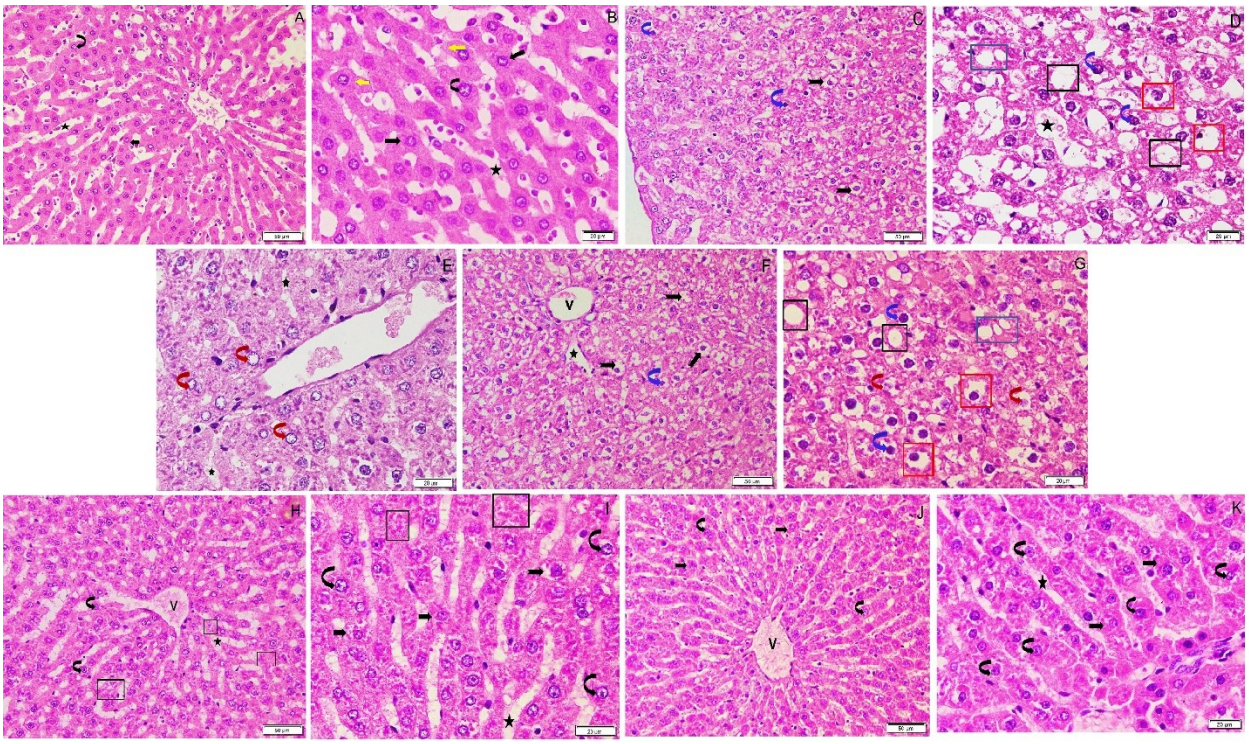

Figure 1. Photomicrographs of rat liver sections stained with H&E. **A, B.** Livers of control rats present hepatocytes arranged in typical radiating cords. Hepatocytes have a central pale nucleus (curved arrow) and eosinophilic cytoplasm (arrow) with clear cell boundaries (yellow arrow). Hepatic sinusoids are located between the plates of hepatocytes (asterisk). **C–E.** Livers of rats from EXIa (HFHF) subgroup exhibit hepatocytes with vacuolated cytoplasm (thick arrows) and either multiple vacuoles separated by thin cytoplasmic threads (blue box) or a single large vacuole (red boxes). Some cells have dark pyknotic nuclei (blue curved arrows), other cells without nuclei (black boxes). Some cells have vacuolated nuclei (red curved arrows). Hepatic sinusoids are dilated (asterisk). **F, G.** Liver of the EXIb (Recovery subgroup) rat showing loss of normal architecture. Large hepatocytes with vacuolated cytoplasm (black arrows) can be seen with multiple vacuoles separated by thin cytoplasmic threads (blue box) or a single large vacuole (red boxes). The nuclei show some irregularity in their outline (blue curved arrow). Hepatocytes exhibit either dark nuclei (blue-curved arrows) or nuclear ghosts (red-curved arrows). Areas without nuclei can be seen (black boxes). Note, the dilatation in the central vein (v). **H, I.** Liver of rat from EXII (HFHF + Rapamycin) subgroup exhibits a classical pattern of hepatocytes' plated radiating from the central vein (v). Majority of hepatocytes demonstrate a pale nucleus with prominent nucleolus (curved arrows) and pale eosinophilic cytoplasm (arrows). Some hepatocytes have vacuolated cytoplasm (black arrows), other areas without nuclei (black box). Non-congested blood sinusoids (asterisk) are noted in between hepatocytes' plates. **J, K.** Livers of EXIII (HFHF + IF) subgroup rats present normal lobular structure

with non-dilated blood sinusoids (asterisk) radiating from the central vein (v). Magnifications: A, C, F, H, J — 200×; B, D, E, G, I, K — 400×.

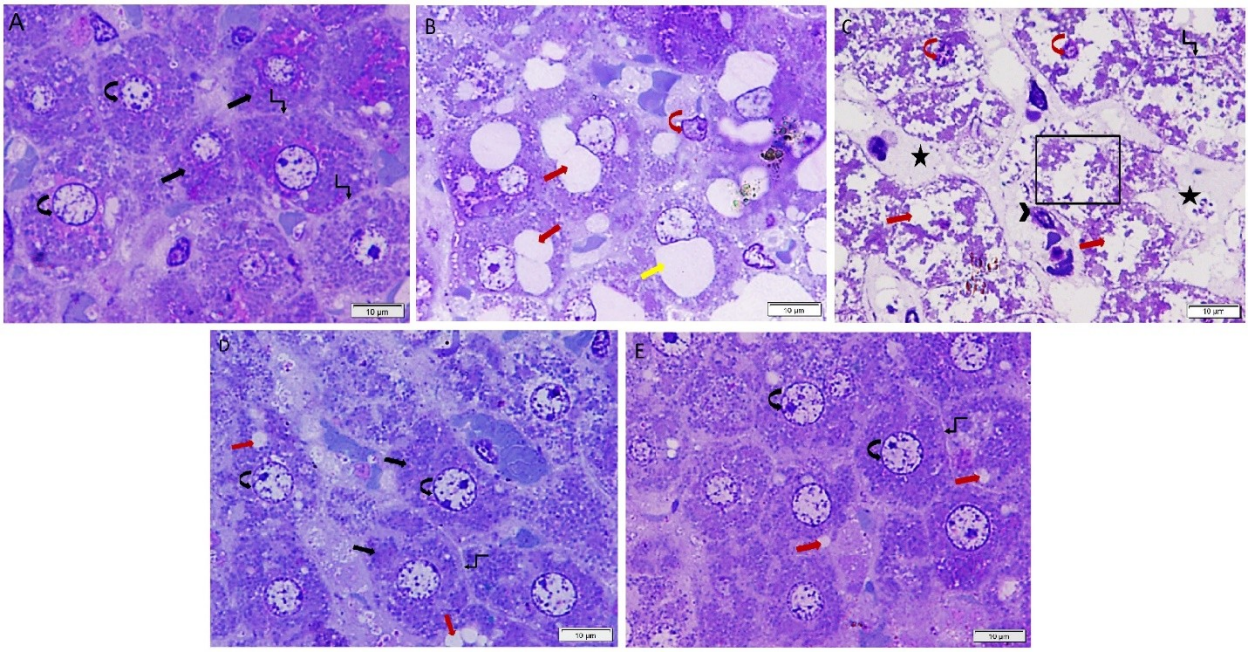

Figure 2. Photomicrograph of semithin sections stained with Toluidine blue. **A.** Liver of control rat reveals hepatocytes with a pale nucleus, prominent nucleolus, and thin nuclear envelope (curved arrows). Granular cytoplasm (arrows) with clear cell boundaries (kinked arrows) are noted. **B.** Liver of rat from EXIa (HFHF subgroup) group shows large rounded, oval, or irregular vacuoles in the hepatocytes' cytoplasm, compressing the nucleus (red curved arrow). The vacuoles are either single and large within the cells (yellow arrow) or multiple smaller and separated by thin cytoplasmic threads (red arrows). **C.** Liver of rat from EXIb (Recovery subgroup) group contains hepatocytes with a dark shrunken nuclei and thick nuclear envelopes (red curved arrows). Extensive cytoplasmic vacuolation results from the presence of many vacuoles, some of them interconnected and of irregular shape (red arrows). Dilated blood sinusoids (asterisks) lined with endothelial cells (arrowhead). **D, E.** Livers of rats from EXII (HFHF + Rapamycin subgroup) and EXIII (HFHF + IF subgroup) groups reveal hepatocytes having regular cell boundaries (kinked arrow), granular cytoplasm (arrows), pale nuclei with the prominent nucleolus, and regular outline of nuclear envelope (curved arrows). Few hepatocytes demonstrate small, dispersed vacuoles (red arrows). Space bar: 10 μm.

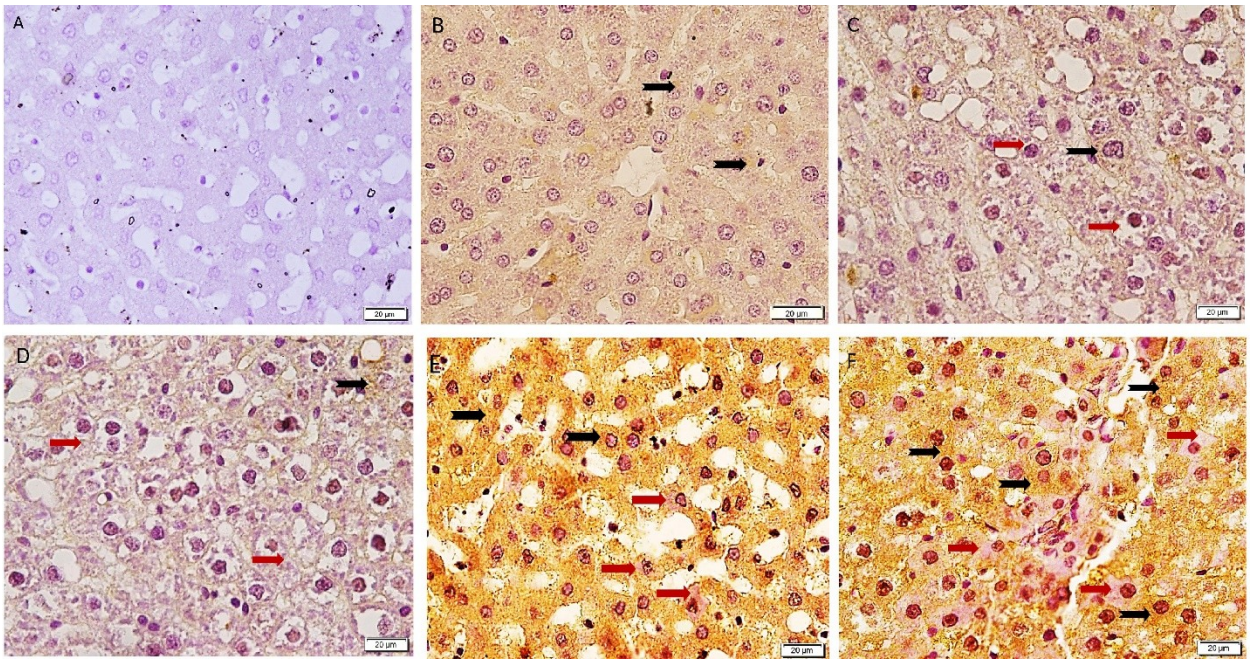

Figure 3. LC3B immunoreactivity in rat liver. **A.** Negative control of rat liver. **B.** Control rat: some hepatocytes show faint cytoplasmic LC3B immunoreactivity to (Ir) (thick arrows). **C, D.** EXIa (HFHF subgroup) and EXIb (Recovery subgroup) groups, respectively: many hepatocytes are negative for LC3B-Ir (red arrows). Few cells show faint cytoplasmic LC3B immunoreactivity (black arrows). **E, F.** In the EXII (HFHF + Rapamycin) and EXIII (HFHF + IF) subgroups, respectively, almost all hepatocytes show strong cytoplasmic LC3B-Ir (black arrows). Few cells exhibit negative cytoplasmic immunoreactivity (red arrows). Magnification: 400×.

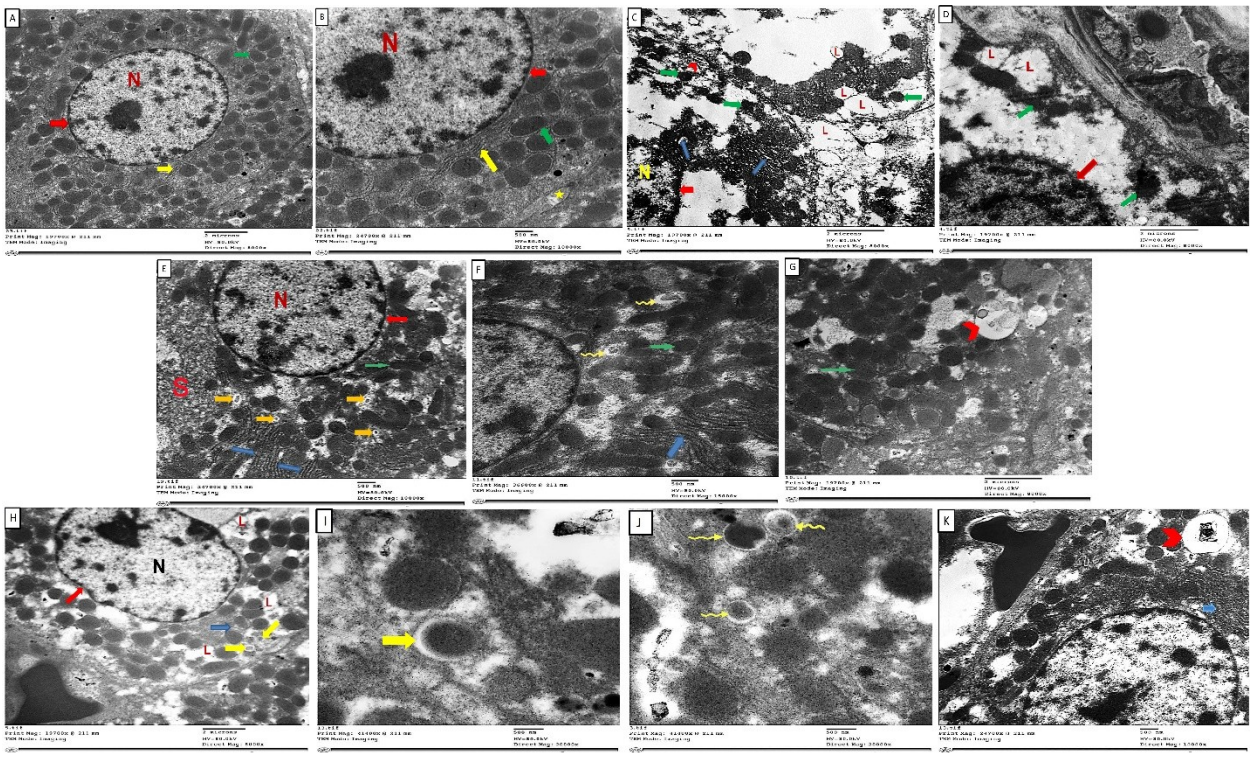

Figure 4. Electron-microscopic photomicrographs of rat liver ultrathin sections. **A, B.** Control group showing hepatocyte with euchromatic nucleus (N) and regular nuclear envelope (red arrows). The hepatocyte has numerous mitochondria (green arrows), and rough endoplasmic reticulum (rER) (yellow arrow). Bile canaliculus with few short microvilli is visible between hepatocytes (yellow star). **C, D.** Livers of rats from EXIa (HFHF subgroup) and EXIb (Recovery subgroup) groups, respectively, exhibit hepatocytes having heterochromatic nucleus (N) with coarse chromatin attached to the inner nuclear membrane (red arrows). Cytoplasm contains multiple lipid droplets (L). Phagolysosome (red arrowhead) and dilated rER cisternae (blue arrows) can be seen. Mitochondria (green arrows) appear shrunken and distorted. **E–G.** Livers of rats of the EXII (HFHF + Rapamycin) subgroup reveal hepatocytes with euchromatic nuclei and prominent nucleoli (N) with regular nuclear envelope (red arrow). Many autophagosomes present in cytoplasm appear as double membrane structures (yellow arrows). rER (blue arrows), SER cisternae (S) and many mitochondria (green arrows) are seen. The stage of phagophore formation (yellow wavy arrows) and autophagosome-containing lipid droplets (red arrowhead) are visible. **H–K.** Livers of rats of the EXIII (HFHF + IF) subgroup contain hepatocytes with euchromatic nuclei (N) and regular nuclear envelope (red arrow). Cytoplasm has some lipid droplets (L), and rER (blue arrow). Some autophagosomes appear as double membraned structures (yellow arrows) with the presence of phagophores (yellow wavy arrows). A phagolysosome with materials left from cellular digestion (red arrowhead) can be demonstrated. Magnifications: A, C, D, G, H — 8000×; B, E, K — 10000×; F — 15000×; I, J — 20000×.

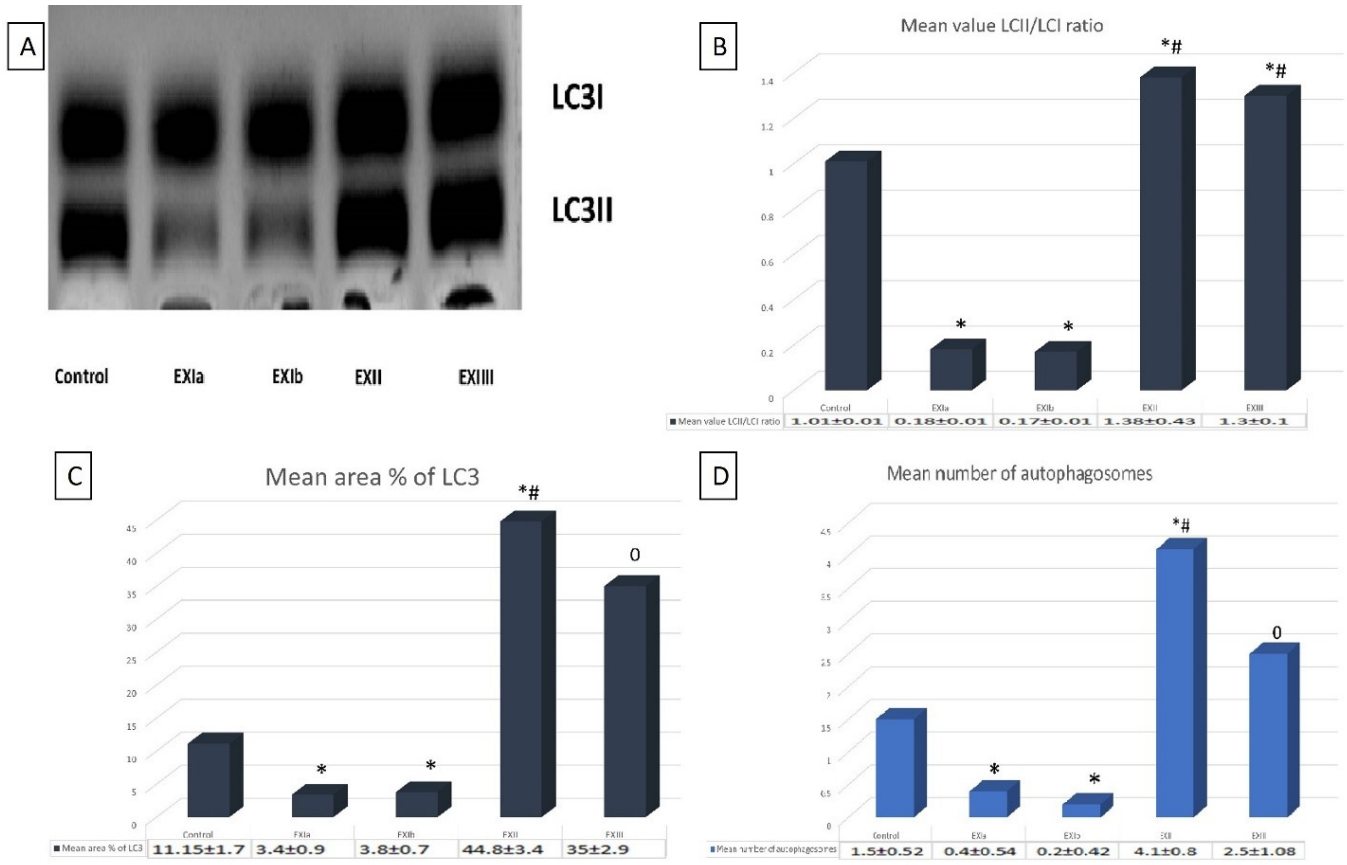

Figure 5. Values of LCII/LCI, mean area of LC3B immunostaining and mean number of autophagosomes/cells. **A.** Western blots of LC3B in the control and experimental groups. **B.** Histogram showing the values of LCII/LCI in the control and experimental groups. **C.** Histogram comparing the mean area% of LC3B immunoreactivity in all groups. **D.** Histogram comparing the mean number of autophagosomes/cells in all groups. The values express mean value ± standard deviation: *Significant compared to the control group ($P < 0.05$). $^{\#}$Significant compared to subgroups EXIa (HFHF subgroup) and EXIb (Recovery subgroup) $P < 0.05$. ^{0}Significant compared to control group & subgroups EXIa (HFHF subgroup), EXIb (Recovery subgroup) and EXII (HFHF + Rapamycin subgroup) $P < 0.05$.